Check for updates

AGU ADVANCING EARTH AND SPACE SCIENCES

Geophysical Research Letters

RESEARCH LETTER
10.1029/2024GL113972

Analysis of Stress in the Cohesive Zone, Dissipation and Fracture Energy During Shear Rupture Experiments

Nicolas Brantut[1]

[1]Department of Earth Sciences, University College London, London, UK Now at GFZ Helmholtz Centre for Geosciences, Potsdam, Germany

Key Points:

- Stress change in cohesive zone can be computed from laboratory rupture experiments
- Stress in cohesive zone is complex for slow ruptures
- Rupture energy budget is consistent with dynamics, despite complexity in slip rate

Supporting Information:

Supporting Information may be found in the online version of this article.

Correspondence to:

N. Brantut,
nicolas.brantut@normalesup.org

Citation:

Brantut, N. (2025). Analysis of stress in the cohesive zone, dissipation and fracture energy during shear rupture experiments. *Geophysical Research Letters*, *52*, e2024GL113972. https://doi.org/10.1029/2024GL113972

Received 4 DEC 2024
Accepted 14 APR 2025

Abstract We analyze high resolution slip rate data obtained during dynamic shear rupture experiments by Berman et al. (2020), https://doi.org/10.1103/physrevlett.125.125503. We use an inverse method to extract the details of strength evolution within the cohesive zone. The overall behavior is slip-weakening at high rupture speeds ($>0.76C_R$, where C_R is the Rayleigh wavespeed), but non-monotonic at low rupture speeds ($<0.76C_R$), with a transient increase after an initial strong weakening. The slower ruptures are associated to more weakening in the cohesive zone. The fraction of breakdown work associated to the initial weakening, immediately behind the rupture tip, matches the fracture energy estimated by independent methods, but the total breakdown work can be much larger than fracture energy. Complex stress evolution in the cohesive zone is compatible with a well-defined fracture energy that explains rupture tip propagation, but the complexity is reflected in local slip rates that will impact radiated waves.

Plain Language Summary Ground motion during earthquakes is determined by the dynamics of fault slip at the earthquake source. An attractive approach to understand how faults slip and eventually generate seismic waves is to consider tectonic faults as thin fractures that propagate in an elastic material, so that existing knowledge on engineering fracture mechanics can be applied. This approach can be tested in the laboratory, and is typically shown to be successful. Here, we analyze recent laboratory data that show interesting departures from classical theory, and specifically determine the details of stress evolution during the slip propagation process. This analysis reveals that in some circumstances (here, for slow ruptures) the stress evolution is more complex than anticipated, which explains why the observed slip rate is markedly different from classical predictions. We show that this complexity is not necessarily incompatible with other predictions from fracture mechanics, notably in terms of energy balance.

1. Introduction

Can we use the theory of linear elastic fracture mechanics (LEFM) to describe earthquakes? This question has received considerable attention over the past decades, not least because LEFM provides tools to reduce the complex problem of earthquake propagation and arrest to that of an (hopefully simpler) energy balance problem that yields a so-called "rupture tip equation of motion" (e.g., Husseini, 1977). Historically, earthquake sources have been modeled using LEFM (e.g., Kostrov, 1966; Madariaga, 1977; Freund, 1979, among many others), whereby the sliding region of an expanding rupture is assumed to sustain a uniform stress, and the potential nonlinearities occurring at the rupture tip where stress drops from a possibly finite peak strength to a constant residual are lumped into a scalar quantity called fracture energy. This description is only valid if the small-scale yielding hypothesis is satisfied, that is, if the nonlinear region, also called the cohesive zone, is small compared to the total rupture size, and if no further changes in strength occur beyond the cohesive zone. Models that include a complete description of the cohesive zone are formally equivalent to LEFM in this case (e.g., Ida, 1972; Palmer & Rice, 1973; Rice, 1968).

However, it is not obvious a priori that the small-scale yielding hypothesis is correct for earthquakes (e.g., Kammer et al., 2023), or more generally for shear ruptures in materials, and if it is sufficient to describe most aspects of rupture dynamics. Indeed, the details of the strength degradation along faults are challenging to access. Only limited information can be accessed from seismological records, because of sparse data coverage, limited frequency bands and physical trade-offs between dynamic quantities (e.g., Olsen et al., 1997; Peyrat et al., 2001; Tinti et al., 2005; Ruiz & Madariaga, 2011). Laboratory experiments that reproduce rupture propagation with extensive instrumentation have a good potential to constrain dynamic stress changes during shear ruptures. It has

© 2025. The Author(s).
This is an open access article under the terms of the Creative Commons Attribution License, which permits use, distribution and reproduction in any medium, provided the original work is properly cited.

19448007, 2025, 9, Downloaded from https://agupubs.onlinelibrary.wiley.com/doi/10.1029/2024GL113972 by Helmholtz-Zentrum Potsdam GFZ, Wiley Online Library on [03/07/2025]. See the Terms and Conditions (https://onlinelibrary.wiley.com/terms-and-conditions) on Wiley Online Library for rules of use; OA articles are governed by the applicable Creative Commons License

been shown that LEFM is good model for the onset of slip at interfaces between elastic bodies (e.g., Svetlizky et al., 2019), in the sense that it correctly predicts rupture tip stress fields (e.g., Kammer & McLaskey, 2019; Svetlizky & Fineberg, 2014) and the motion of the rupture tip (e.g., Bayart et al., 2016; Ben-David et al., 2010). Despite this success, in most laboratory experiments the cohesive zone remains elusive: it is typically small (from mm to cm) and transient (duration of the order of microseconds), and can only be observed if stress measurements are made directly on the fault, or extremely close to it (typically at distances much smaller than the cohesive zone size itself; see Text S1 in Supporting Information S1). Most experimental data are not able to resolve any cohesive zone detail because measurements are made at some distance from the fault plane (e.g., Johnson & Scholz, 1976; Ohnaka et al., 1987; Okubo & Dieterich, 1984; Svetlizky & Fineberg, 2014). A few recent experimental studies where some details of the stress evolution could be resolved (e.g., Kammer & McLaskey, 2019; Paglialunga et al., 2022; Rubino et al., 2017) show that the cohesive zone can be more complex than previously assumed.

Experimental work by Paglialunga et al. (2022) showed that multistage weakening can lead to the existence of several fracture energy values, appropriate for different stages of the rupture process. Using full-field imaging techniques during dynamic rupture experiments, Rubino et al. (2022) showed that slip between elastic blocks occurs in bursts with highly variable slip rate and traction evolution, which is at odds with the crack-like ruptures typically expected in the LEFM approximation. The slip rate evolution along the fault is what determines near field strong motion and overall earthquake source-time functions, and it is thus important to determine if and how slip rate variations arise during dynamic fault motion.

In a recent study, Berman et al. (2020) reported slip rate data obtained during spontaneous dynamic propagation of shear cracks along a preexisting interface in Polymethylmethacrylate (PMMA). In their original paper, both LEFM and a simple cohesive zone model (a monotonically decreasing strength behind the rupture tip) were used to interpret the data. Their main conclusion was that LEFM predictions are a good match to slip rate data measured in fast ruptures, $C_f \geq 0.8C_R$, where C_f is the rupture speed and C_R is the Rayleigh wave speed, and that a simple regularization of the LEFM tip singularity by the cohesive zone model

$$\tau(x) = (\tau_p - \tau_r)\, e^{-x/x_c} + \tau_r \tag{1}$$

produces a good match to the entire slip rate evolution behind the tip. In Equation 1, τ_p refers to the peak strength and τ_r denotes the residual strength of the interface, x is the along-fault coordinate, and the quantity x_c is the characteristic size of the cohesive zone.

However, neither LEFM nor Equation 1 produced a satisfying match to slip rate data obtained in "slow" ruptures, $C_f < 0.8C_R$, despite the overall good match of LEFM with "far-field" strain data. The complexity in slip rate evolution (Figure 4 of Berman et al., 2020) clearly calls for an equally complex strength evolution within the cohesive zone.

Here, we use Berman et al.'s high resolution slip rate data in an inverse problem to determine the cohesive strength. This approach allows us to systematically explore the features of the cohesive strength that produce the observed slip rate, and determine the key differences between slow and fast ruptures. In addition, we use our estimate of strength evolution to determine the energy dissipation (specifically, the breakdown work (Tinti et al., 2005)), and compare it with independent estimates of fracture energy. Overall, we find that slow ruptures tend to have a complex stress evolution, which includes substantial strengthening. Despite that complexity, the breakdown work matches well with the elastically inferred fracture energy. Thus, LEFM seems to be a good approximation in terms of energy balance, but cohesive zone complexity leads to clear differences in local slip rate evolution.

2. Method

The data used are the slip rate profiles and rupture speeds from Berman et al. (2020) determined by optical methods during dynamic ruptures running along a PMMA interface. In their experiments, Berman et al. (2020) sheared a narrow (5.5 mm) slab of PMMA (length 150 mm) on top of a PMMA base, and determined rupture tip position and speed by optically imaging the real area of contact between the blocks. An array of strain gauges positioned 3.5 mm away from the surface was used to measure dynamic strains (and obtain fracture energy of each

19448007, 2025, 9, Downloaded from https://agupubs.onlinelibrary.wiley.com/doi/10.1029/2024GL113972 by Helmholtz-Zentrum Potsdam GFZ, Wiley Online Library on [03/07/2025]. See the Terms and Conditions (https://onlinelibrary.wiley.com/terms-and-conditions) on Wiley Online Library for rules of use; OA articles are governed by the applicable Creative Commons License

rupture), and a dedicated optical interferometer was developed to measure slip and slip rate on a small patch (5 mm in length) along the fault. Details of the experimental setup and measurement methods are given in the original work of Berman et al. (2020). Note that Berman et al. (2020) report their results in terms of particle velocity v_x, which ought to be multiplied by 2 to obtain the slip rate.

The material surrounding the interface is assumed to be linear elastic. We are only interested in the near-tip region, and thus consider the approximation where the rupture is semi-infinite, that is, the other rupture tip is far, driven by a negligible stress drop. We also follow the original analysis of Berman et al. (2020) and assume the rupture is locally at steady-state (constant rupture speed). Elastodynamic equilibrium implies a relationship between slip rate V and shear stress τ in the rupturing patch (e.g., Viesca & Garagash, 2015):

$$\tau(x) - \tau_{\mathrm{b}} = \frac{\bar{\mu}}{2\pi C_{\mathrm{f}}} \int_0^{\infty} \frac{V(\xi)}{\xi - x} d\xi, \tag{2}$$

where x is the position along the rupture ($x = 0$ at the tip), τ_{b} is the background stress, and $\bar{\mu}$ is a modified shear modulus that depends on the rupture speed C_{f}. In mode II, we have (Rice et al., 2005)

$$\bar{\mu} = \frac{\mu}{1-\nu} \times \frac{4\alpha_{\mathrm{s}}\alpha_{\mathrm{d}} - \left(1+\alpha_{\mathrm{s}}^2\right)^2}{\alpha_{\mathrm{s}}\left(1-\alpha_{\mathrm{s}}^2\right)}, \tag{3}$$

where $\alpha_{\mathrm{s,d}} = \sqrt{1 - \left(C_{\mathrm{f}}/C_{\mathrm{s,d}}\right)^2}$, with C_{s} and C_{d} the S and P wave speeds of the surrounding material.

It is tempting to use Equation 2 directly, using the slip rate obtained in the experiments and computing the integral to obtain the shear stress. However, this strategy is impractical: The upper integration bound should extend to infinity, but the slip rate data only span a narrow region near the tip, so the integral cannot be computed unless we severely extrapolate the slip rate data. The alternative strategy used here is to determine $\tau(x)$ via an inverse method.

We assume $\tau(x)$ to be a piece-wise linear function, parameterized by its value τ_i at a set of fixed positions x_i ($i = 0, \ldots, N$), valid for $x \in (0, +\infty)$:

$$\tau(x) = \begin{cases} \tau_{i-1} + (\tau_i - \tau_{i-1})(x - x_{i-1})/(x_i - x_{i-1}) & \text{if } x \in [x_{i-1}, x_i], \\ \tau_N & \text{if } x > x_N, \end{cases} \tag{4}$$

where $x_0 = 0$ and x_N is the maximum position where slip rate was recorded. The shear stress τ_N is imposed at all positions beyond x_N, which means that τ_N is a constant residual stress. To ensure consistency with the semi-infinite crack approximation, the residual stress τ_N is imposed equal to the background stress τ_{b}. The unknowns of our problem are thus the values of τ_i at all positions x_i.

As our forward problem, we use the stress evolution (Equation 4) to compute the associated slip rate from (Equation 2), which can be done numerically using Gauss-Chebyshev quadrature (Viesca & Garagash, 2018). The inverse problem is solved by the quasi-Newton method (Tarantola, 2005). The details of the inversion procedure are given in Text S2 in Supporting Information S1. For each slip rate profile, we obtain a mean model (in the least squares sense) for the best-fitting shear stress profile. Synthetic tests show that the results are not sensitive to the detailed choice of rupture tip position, and that the inverted shear stress profile is only constrained up to a constant, uniform background (see Text S3 in Supporting Information S1).

3. Results

Representative examples of slip rate fits and corresponding shear stress are given in Figure 1. As originally reported by Berman et al. (2020), there is a clear difference between slow $\left(C_{\mathrm{f}} < 0.76 C_{\mathrm{R}}\right)$ and fast cracks: slow ruptures tend to be associated with nonlinear and nonmonotonic traction evolution. The two slip rate peaks occurring during slow ruptures appear to be linked to a two-stage weakening, with an initial rapid stress drop, followed by a slower decay. The increase in slip rate at some distance from the tip is explained by a stress rebound

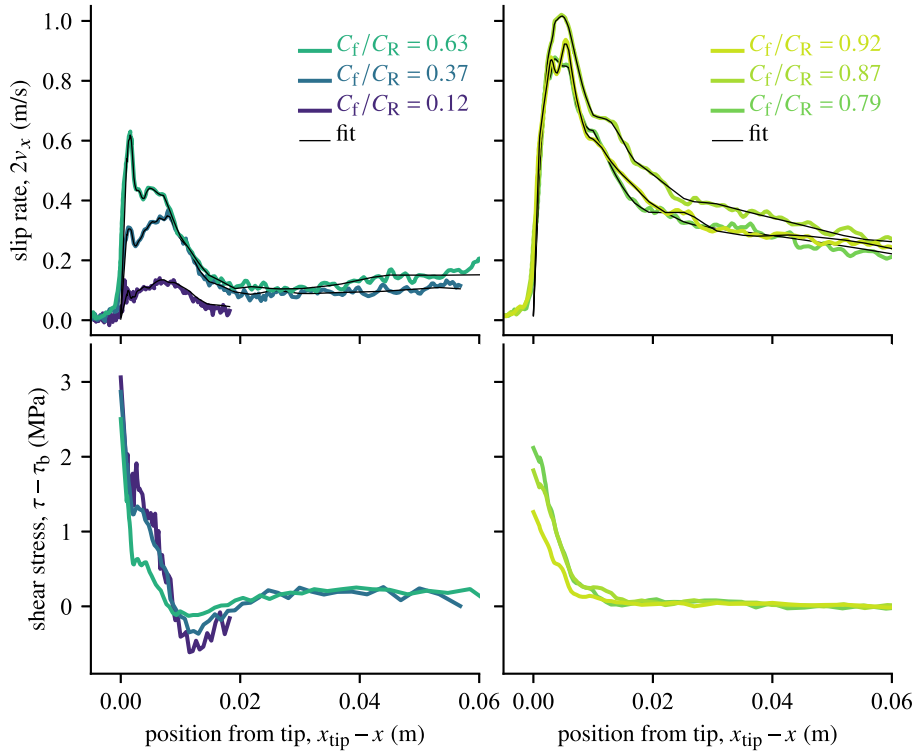

Figure 1. Examples of shear stress evolution inverted from slip rate profiles.

(strengthening). By contrast, fast ruptures are associated to very simple traction evolution, a monotonic, almost linear weakening behavior with constant residual stress.

The shear stress profiles along the crack can be plotted as a function of slip (Figure 2). The behavior is different between slow and fast cracks, with slow ruptures associated with restrengthening at around 8 μm slip. In those slow ruptures, the shear stress peaks at about 3 MPa above the background stress, then drops below τ_b (i.e., strong dynamic strength drop), and finally recover. At large slip, the strength approaches a constant as the interface gradually restrengthens, but it is not certain that a constant residual is achieved fully. One important feature of the slip rate evolution, the existence of a first peak followed by a second, more gradual "bump", is specifically caused

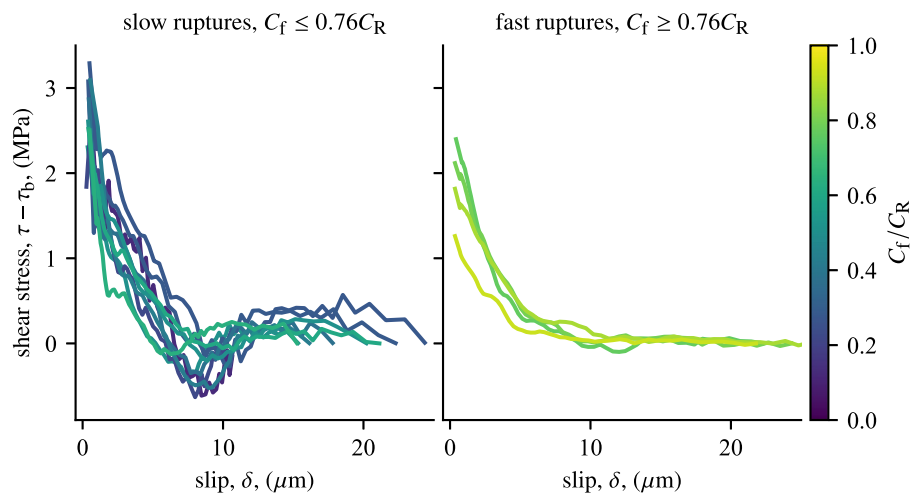

Figure 2. Shear stress evolution vs. slip obtained from inversion of slip rate profiles.

19448007, 2025, 9, Downloaded from https://agupubs.onlinelibrary.wiley.com/doi/10.1029/2024GL113972 by Helmholtz-Zentrum Potsdam GFZ, Wiley Online Library on [03/07/2025]. See the Terms and Conditions (https://onlinelibrary.wiley.com/terms-and-conditions) on Wiley Online Library for rules of use; OA articles are governed by the applicable Creative Commons License

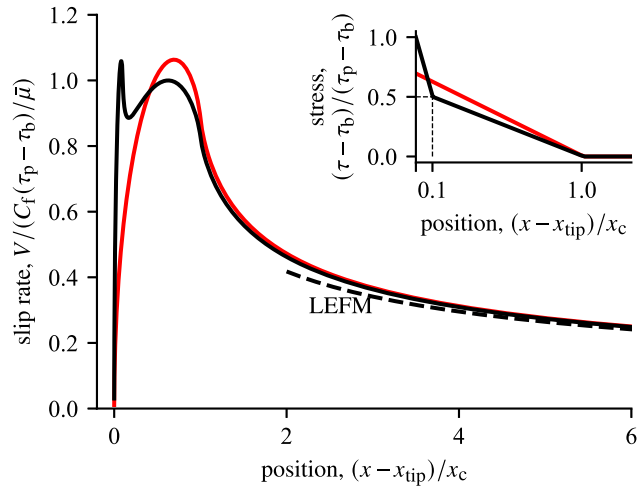

Figure 3. Typical slip rate profile obtained from two successive weakening stages in a semi-inifinite, dynamically progating crack solution (Equation 2). The background stress is assumed equal to the residual strength. The strength decreases sharply from a peak value τ_p down to $\tau_p/2$ over a distance $x_c/10$, and then decreases slowly down to the residual at a distance x_c from the tip (inset). The dashed line shows the slip rate obtained from the linear elastic fracture mechanics limit with a fracture energy consistent with the slip-weakening behavior. For comparison, the slip rate associated to a single linear weakening stage (with the same fracture energy) is shown in red.

by the presence of two weakening stages: An initial rapid weakening, typically occurring over the first 1 μm of slip followed by a more gradual one, as can be confirmed by independent forward simulations (Figure 3).

By contrast, consistently with the original work of Berman et al. (2020), the slip rate during fast ruptures is explained by a monotonic decay of strength and stabilization to a constant residual. The details of stress evolution revealed by the inversion method show that one of the fast ruptures (at $C_f/C_R = 0.87$) also includes a short, fast initial weakening stage within the first 0.5 μm of slip (Figure 2). This indicates that the two-stage weakening might persist even at high rupture (and slip) velocities, but might be less visible due to a vanishing difference between the two stages.

An interesting quantity that can be computed from the stress evolution is the so-called "breakdown work" (e.g., Tinti et al., 2005). For nonmonotonic shear stress versus slip behavior, the breakdown work can be defined as

$$E_{BD} = \int_0^{\delta} \tau(\delta') - \tau_{min} d\delta', \tag{5}$$

where τ_{min} is the minimum stress reached in the interval $(0, \delta)$. The breakdown work is (by this definition) an increasing function of cumulated slip. We observe a stabilization of breakdown work for fast ruptures (Figure 4a). For slow ruptures, the breakdown work reaches a plateau when restrengthening occurs (at around 8 μm slip), and keeps increasing beyond that point: there is more dissipation away from the crack tip.

We can also use the breakdown work to estimate the fracture energy Γ. For slip-weakening cohesive laws with a well-defined residual, the fracture energy is the limit of E_{BD} at large slip (Palmer & Rice, 1973). For non-monotonic cohesive law, we may identify Γ with the "near-tip" dissipation, that is, the fraction of E_{BD} that is associated with the initial weakening, down to the minimum stress achieved along the crack. The fracture energy estimated this way (Figure 4b) is of similar magnitude and decreases with increasing rupture speed in a similar way to that determined by Berman et al. (2020) based on strain gauge data fitted to a singular crack tip stress field (their Figure S4).

4. Discussion and Conclusions

The present analysis brings quantitative constraints to the main result obtained by Berman et al. (2020): slow ruptures are characterized by slip rate profiles that are markedly different from the predictions of LEFM and from

19448007, 2025, 9, Downloaded from https://agupubs.onlinelibrary.wiley.com/doi/10.1029/2024GL113972 by Helmholtz-Zentrum Potsdam GFZ, Wiley Online Library on [03/07/2025]. See the Terms and Conditions (https://onlinelibrary.wiley.com/terms-and-conditions) on Wiley Online Library for rules of use; OA articles are governed by the applicable Creative Commons License

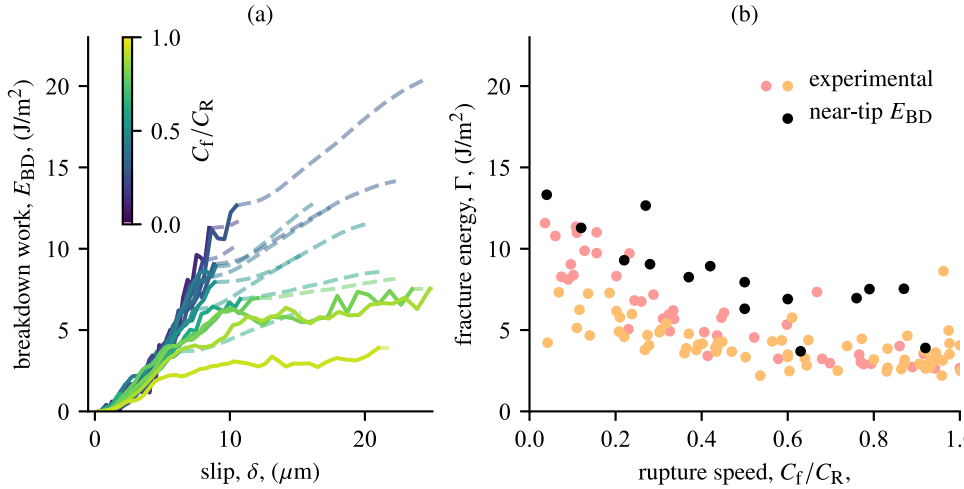

Figure 4. (a) Energy dissipation, and (b) estimate of fracture energy from the inverted shear stress evolution. The dashed portions of curves in (a) correspond to the restrengthening phase of the stress-slip evolution. Black dots in (b) correspond to fracture energy estimated using the inverted stress-slip curves, pink and orange dots are independent estimates made by Berman et al. (2020) based on strain gauge measurements (fitting of stress variations during rupture assuming singular rupture). The two colors correspond to two experiments conducted in the same conditions.

simple weakening cohesive laws. Indeed, for ruptures where $C_f < 0.76C_R$, the inversion procedure shows that shear stress initially decreases, reaches a minimum, but increases again. This observation is systematic, and different from what happens in fast cracks. In addition, the presence of two separate slip rate peaks shows that weakening occurs in two stages, with an initial abrupt drop followed by a slower decrease (confirmed by simulations, see Figure 3).

A two-stage weakening was already inferred from near-fault stress measurements in similar experiments by (Paglialunga et al., 2022), but its impact on slip rate in the cohesive zone is now clearly measured. The physics of weakening in PMMA is obviously different from that in rocks in natural fault zones, but multi-stage weakening is a likely possibility in natural earthquakes due to existence of a series of weakening processes, from flash heating, thermal pressurization (e.g., Noda et al., 2009; Viesca & Garagash, 2015), thermal weakening (e.g., Harbord et al., 2021; Hirose & Shimamoto, 2005), coupled to fluid dilatancy and diffusion effects (Brantut, 2021). As predicted by LEFM, the effect of two-stage weakening is restricted to the cohesive zone, and the expected classical solution (with a decay proportional to $1/\sqrt{x - x_{tip}}$) should emerge at large distances to the tip (Figure 3, dashed lines). In the data set from Berman et al., the slip rate for slow ruptures is different from that limit due to a restrengthening effect.

The cause of strengthening in the cohesive zone at low rupture speed is not clear. Polymethylmethacrylate has a very low melting temperature (only around 120 K above ambient temperature), and it is possible that local melting at asperity contacts occurred during the tests reported by Berman et al. (2020). In rocks, the onset of melting during high velocity friction tests is often associated with a transient strengthening, leading to the so-called "viscous break" effect (Hirose & Shimamoto, 2005); this process might have occurred in the PMMA experiments. Such nonmonotonic strength evolution was not observed in similar rupture experiments conducted in Homalite (Rubino et al., 2017), which displayed only monotonic weakening with ongoing slip that could be explained quantitatively by flash heating (Rice, 2006). By contrast, recent work on fault gouge by (Rubino et al., 2022) also showed slip-strengthening behavior at low slip rate. Thus, it is likely that the details of the cohesive zone exhibited here are material-dependent or microstructure-dependent. For natural earthquakes, strength recovery at some distance from the rupture front could occur due to late-stage melting (viscous break effect) or strength recovery due to the decrease in slip rate as would be predicted by flash heating (e.g., Harbord et al., 2021). Such restrengthening may have important consequences for the dynamics of rupture and earthquake scaling laws (e.g., Gabriel et al., 2024).

One counterintuitive aspect of the strength evolution inverted from slip rate data is that more weakening is observed during slow rupture compared to fast ruptures (Figure 2), which translates into more weakening at low slip rate (Figure 5). The shear stress evolution within the cohesive zone can be interpreted qualitatively in terms of

19448007, 2025, 9, Downloaded from https://agupubs.onlinelibrary.wiley.com/doi/10.1029/2024GL113972 by Helmholtz-Zentrum Potsdam GFZ, Wiley Online Library on [03/07/2025]. See the Terms and Conditions (https://onlinelibrary.wiley.com/terms-and-conditions) on Wiley Online Library for rules of use; OA articles are governed by the applicable Creative Commons License

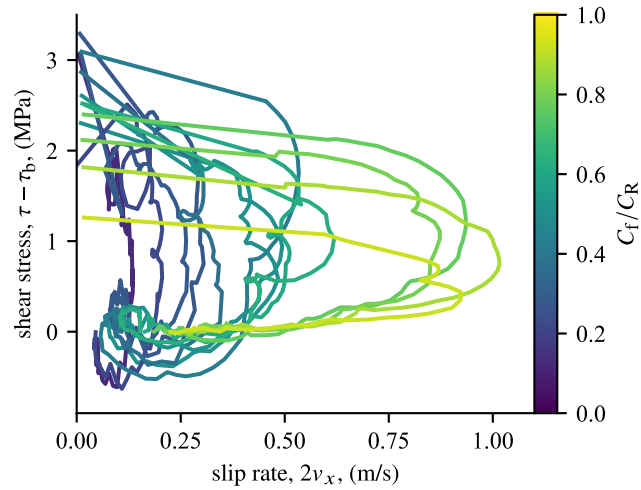

Figure 5. Cohesive zone stress evolution as a function of slip rate.

a competition between the so-called "direct effect" in rate and state friction (Dieterich, 1979; Ruina, 1983), which produces an instantaneous strengthening upon slip acceleration, and the evolution of one or several internal state variables that characterize the microstructure of the interface, which here produce weakening. An analysis of shear crack propagation with rate-and-state friction as constitutive law in the cohesive zone, given by Garagash (2021), demonstrates that one expects increasing strength drop and larger fracture energy with increasing rupture speed, in contrast to the observations of Figures 4 and 5. Therefore, the conventional rate-and-state framework (with a single state variable) is not a priori consistent with the PMMA experiments. A few possibilities might be envisioned to explain the data. There might exist a true threshold in slip rate (and hence in rupture speed) above which the frictional behavior of PMMA changes character, which could be consistent with flash heating or frictional melting (as reported originally by Berman et al. (2020)). This option is akin to modeling friction in the cohesive zone with two or more state variables, each having independent dependencies on slip and slip rate, possibly activated by temperature. There might also be an effect of prior state, whereby fast ruptures tend to occur along interfaces that experienced less contact healing (i.e., the initial strength is far from steady state). In this case, one would expect an effect of the particular rupture sequence in the experiments, which was not documented by Berman et al. (2020).

The details of the cohesive zone revealed by the inverse model illustrate a crucial phenomenon in fracture mechanics that could be overlooked if we focus only on the local friction law of the material: more weakening in the cohesive zone does not necessarily imply faster rupture speeds. Here, the opposite is observed. This observation can be explained by considering that the fracture energy associated with slower events seems larger than, or at best of similar magnitude to, that associated to faster events (Figure 4). We thus observe directly the disconnect between the details of the weakening in the cohesive zone and fracture energy, which is an integrated quantity that drives rupture propagation and is insensitive to such details. The complex cohesive law is not in contradiction with the existence of a well-defined fracture energy and LEFM behavior at scales much larger than that of the cohesive zone.

It is difficult to make a clear sense of the breakdown work as defined in (Equation 5) beyond the minimum stress achieved in the cohesive zone (Figure 4a, dashed lines): this energy keeps increasing with increasing slip, and we see a clear disconnect between the fracture energy that drives the rupture (edge-localized dissipation) and the overall dissipation in the interior of the growing rupture. What cannot be addressed with the existing dataset is whether the stress would continue to rise well beyond the tip region, or if more weakening occurs. The stress evolution away from the rupture tip contributes to the energy release rate and thus to the overall dynamics of rupture, especially during rupture arrest (e.g., Paglialunga et al., 2022).

In conclusion, the complex stress evolution inferred during "slow" ruptures $\left(C_f < 0.76C_R\right)$ along PMMA interfaces highlights that there might be regimes where LEFM is only applicable in an "effective" sense: one can use LEFM concepts (fracture energy) to understand, to first order, the dynamics of rupture expansion, but using

19448007, 2025, 9, Downloaded from https://agupubs.onlinelibrary.wiley.com/doi/10.1029/2024GL113972 by Helmholtz-Zentrum Potsdam GFZ, Wiley Online Library on [03/07/2025]. See the Terms and Conditions (https://onlinelibrary.wiley.com/terms-and-conditions) on Wiley Online Library for rules of use; OA articles are governed by the applicable Creative Commons License

physical quantities that are not necessarily well-defined material parameters. In this sense, the fracture energy derived here for slow ruptures (Figure 4b) is the "effective" energy that would produce similar dynamics to that of an ideal LEFM rupture, but does not capture all aspects of that rupture. In particular, the slip rate evolution is critically dependent on details of the cohesive zone not captured by LEFM. This has implications for earthquakes: the slip rate history on the rupture plane (source-time function) is what determines ground shaking and the far-field radiation measured in seismograms, and it remains to be seen to which extent LEFM (or a modification thereof) can capture both earthquake propagation and radiation.

Data Availability Statement

No new data have been generated in this work. Existing data from Berman et al. (2020) were used.

Acknowledgments
I thank Fabian Barras, Neri Berman, Jay Fineberg, Federica Paglialunga and François Passelègue for key discussions and feedback during the (long) preparation of this manuscript. Comments by Dmitry Garagash and an anonymous reviewer helped clarify many points of the paper. Rob Viesca helped clarify some review comments. Funding from the UK Natural Environment Research Council (Grant NE/S000852/1), the European Research Council under the European Union's Horizon 2020 research and innovation programme (project RockDeaf, Grant agreement 804685; project RockDeath, Grant agreement 101088963), and a Philip Leverhulme Prize from the Leverhulme Trust, is gratefully acknowledged.

References

Bayart, E., Svetlizky, I., & Fineberg, J. (2016). Fracture mechanics determine the lengths of interface ruptures that mediate frictional motion. *Nature Physics*, *12*(2), 166–170. https://doi.org/10.1038/nphys3539

Ben-David, O., Cohen, G., & Fineberg, J. (2010). The dynamics of the onset of frictional slip. *Science*, *330*(6001), 211–214. https://doi.org/10.1126/science.1194777

Berman, N., Cohen, G., & Fineberg, J. (2020). Dynamics and properties of the cohesive zone in rapid fracture and friction. *Physics Research Letter*, *125*(12), 125–503. https://doi.org/10.1103/PhysRevLett.125.125503

Brantut, N. (2021). Dilatancy toughening of shear cracks and implications for slow rupture propagation. *Journal of Geophysical Research*, *126*(11), e2021JB022239. https://doi.org/10.1029/2021JB022239

Dieterich, J. H. (1979). Modeling of rock friction 1. experimental results and constitutive equations. *Journal of Geophysical Research*, *84*(B5), 2161–2168. https://doi.org/10.1029/jb084ib05p02161

Freund, L. B. (1979). The mechanics of dynamic shear crack propagation. *Journal of Geophysical Research*, *84*(B5), 2199–2209. https://doi.org/10.1029/jb084ib05p02199

Gabriel, A.-A., Garagash, D. I., Palgunadi, K. H., & Mai, P. M. (2024). Fault size-dependent fracture energy explains multiscale seismicity and cascading earthquakes. *Science*, *385*(6707), eadj9587. https://doi.org/10.1126/science.adj9587

Garagash, D. I. (2021). Fracture mechanics of rate-and-state faults and fluid injection induced slip. *Philosophical Transaction Royal Society A*, *379*(2196), 129. 20200. https://doi.org/10.1098/rsta.2020.0129

Harbord, C., Brantut, N., Spagnuolo, E., & Di Toro, G. (2021). Fault friction during simulated seismic slip pulses. *Journal of Geophysical Research*, *126*(8), e2021JB022149. https://doi.org/10.1029/2021JB022149

Hirose, T., & Shimamoto, T. (2005). Growth of molten zone as a mechanism of slip weakening of simulated faults in gabbro during frictional melting. *Journal of Geophysical Research*, *110*(B5), B05202. https://doi.org/10.1029/2004JB003207

Husseini, M. I. (1977). Energy balance for motion along a fault. *Geophysical Journal of the Royal Astronomical Society*, *49*(3), 699–714. https://doi.org/10.1111/j.1365-246x.1977.tb01313.x

Ida, Y. (1972). Cohesive force across the tip of a longitudinal-shear crack and griffith's specific surface energy. *Journal of Geophysical Research*, *77*(20), 3796–3805. https://doi.org/10.1029/jb077i020p03796

Johnson, T. L., & Scholz, C. H. (1976). Dynamics properties of stick-slip friction of rock. *Journal of Geophysical Research*, *81*(5), 881–888. https://doi.org/10.1029/jb081i005p00881

Kammer, D. S., & McLaskey, G. C. (2019). Fracture energy estimates from large-scale laboratory earthquakes. *Earth and Planetary Science Letters*, *511*, 36–43. https://doi.org/10.1016/j.epsl.2019.01.031

Kammer, D. S., McLaskey, G. C., Abercrombie, R. E., Aumpuero, J.-P., Cattania, C., Cocco, M., et al. (2023). Earthquake energy dissipation in a fracture mechanics framework. *Nature Communications*, *15*(1), 4736. https://doi.org/10.1038/s41467-024-47970-6

Kostrov, B. V. (1966). Unsteady propagation of longitudinal shear cracks. *Journal of Applied Mathematics and Mechanics*, *30*(6), 1241–1248. https://doi.org/10.1016/0021-8928(66)90087-6

Madariaga, R. (1977). High-frequency radiation from crack (stress drop) models of earthquake faulting. *Geophysical Journal of the Royal Astronomical Society*, *51*(3), 625–651. https://doi.org/10.1111/j.1365-246x.1977.tb04211.x

Noda, H., Dunham, E. M., & Rice, J. R. (2009). Earthquake ruptures with thermal weakening and the operation of major faults at low overall stress levels. *Journal of Geophysical Research*, *114*(B7), B07302. https://doi.org/10.1029/2008JB006143

Ohnaka, M., Kuwahara, Y., & Yamamoto, K. (1987). Constitutive relations between dynamic physical parameters near a tip of the propagating slip zone during stick-slip shear failure. *Tectonophysics*, *144*(1–3), 109–125. https://doi.org/10.1016/0040-1951(87)90011-4

Okubo, P. G., & Dieterich, J. H. (1984). Effects of physical fault properties on frictional instabilities produced on simulated faults. *Journal of Geophysical Research*, *89*(B7), 5817–5827. https://doi.org/10.1029/jb089ib07p05817

Olsen, K. M., Madariaga, R., & Archuleta, R. J. (1997). Three-dimensional dynamic simulation of the 1992 Landers earthquake. *Science*, *278*(5339), 834–838. https://doi.org/10.1126/science.278.5339.834

Paglialunga, F., Passelègue, F. X., Brantut, N., Barras, F., Lebihain, M., & Violay, M. (2022). On the scale dependence in the dynamics of frictional ruptre: Constant fracture energy versus size-dependent breakdown work. *Earth and Planetary Science Letters*, *584*, 117442.

Palmer, A. C., & Rice, J. R. (1973). The growth of slip surfaces in the progressive failure of over-consolidated clay. *Proceedings of the Royal Society of London A.*, *332*, 527–548.

Peyrat, S., Olsen, K., & Madariaga, R. (2001). Dynamic modeling of the 1992 Landers earthquake. *Journal of Geophysical Research*, *106*(B11), 26467–26482. https://doi.org/10.1029/2001jb000205

Rice, J. R. (1968). Mathematical analysis in the mechanics of fracture. In H. Liebowitz (Ed.), *Fracture: An advanced treatise*, *Mathematical fundamentals* (Vol. 2, pp. 191–311). Academic Press.

Rice, J. R. (2006). Heating and weakening of faults during earthquake slip. *Journal of Geophysical Research*, *111*(B5), B05311. https://doi.org/10.1029/2005JB004006

Rice, J. R., Sammis, C. G., & Parsons, R. (2005). Off-fault secondary failure induced by a dynamic slip pulse. *Bulletin of the Seismological Society of America*, *95*(1), 109–134. https://doi.org/10.1785/0120030166

19448007, 2025, 9, Downloaded from https://agupubs.onlinelibrary.wiley.com/doi/10.1029/2024GL113972 by Helmholtz-Zentrum Potsdam GFZ, Wiley Online Library on [03/07/2025]. See the Terms and Conditions (https://onlinelibrary.wiley.com/terms-and-conditions) on Wiley Online Library for rules of use; OA articles are governed by the applicable Creative Commons License

Rubino, V., Lapusta, N., & Rosakis, A. J. (2022). Intermittent lab earthquakes in dynamically weakening fault gouge. *Nature*, *606*(7916), 922–929. https://doi.org/10.1038/s41586-022-04749-3

Rubino, V., Rosakis, A. J., & Lapusta, N. (2017). Understanding dynamic friction through spontaneously evolving laboratory earthquakes. *Nature Communications*, *8*(1), 15991. https://doi.org/10.1038/ncomms15991

Ruina, A. L. (1983). Slip instability and state variable friction laws. *Journal of Geophysical Research*, *88*(10), 10359. https://doi.org/10.1029/jb088ib12p10359

Ruiz, S., & Madariaga, R. (2011). Determination of the friction parameters of the Mw 6.7 Michilla earthquake in northern Chile by dynamic inversion. *Geophysical Research Letters*, *38*(9), L09317. https://doi.org/10.1029/2011GL047147

Svetlizky, I., Bayart, E., & Fineberg, J. (2019). Brittle fracture theory describes the onset of frictional motion. *Annual Review of Condensed Matter Physics*, *10*(1), 253–273. https://doi.org/10.1146/annurev-conmatphys-031218-013327

Svetlizky, I., & Fineberg, J. (2014). Classical shear cracks drive the onset of dry frictional motion. *Nature*, *509*(7499), 205–208. https://doi.org/10.1038/nature13202

Tarantola, A. (2005). *Inverse problem theory* (2nd ed.). Society for Industrial Mathematics.

Tinti, E., Spudich, P., & Cocco, M. (2005). Earthquake fracture energy inferred from kinematic rupture models on extended faults. *Journal of Geophysical Research*, *110*(B12), B12303. https://doi.org/10.1029/2005JB003644

Viesca, R. C., & Garagash, D. I. (2015). Ubiquitous weakening of faults due to thermal pressurization. *Nature Geoscience*, *8*(11), 875–879. https://doi.org/10.1038/ngeo2554

Viesca, R. C., & Garagash, D. I. (2018). Numerical methods for coupled fracture problems. *Journal of the Mechanics and Physics of Solids*, *113*, 13–34. https://doi.org/10.1016/j.jmps.2018.01.008

References From the Supporting Information

Poliakov, A. N. B., Dmowska, R., & Rice, J. R. (2002). Dynamic shear rupture interactions with fault bends and off-axis secondary faulting. *Journal of Geophysical Research*, *107*(B11), 2295. https://doi.org/10.1029/2001JB000572

Revels, J., Lubin, M., & Papamarkou, T. (2016). Forward-mode automatic differentiation in Julia. *arXiv:1607.07892 [cs.MS]*.

19448007, 2025, 9, Downloaded from https://agupubs.onlinelibrary.wiley.com/doi/10.1029/2024GL113972 by Helmholtz-Zentrum Potsdam GFZ, Wiley Online Library on [03/07/2025]. See the Terms and Conditions (https://onlinelibrary.wiley.com/terms-and-conditions) on Wiley Online Library for rules of use; OA articles are governed by the applicable Creative Commons License